Numerical Heat Transfer, Part A, 36:1–16, 1999
Copyright © 1999 Taylor & Francis
1040–7782 /99 $12.00 + .00

RAYLEIGH-BÉNARD CONVECTION IN LIMITED DOMAINS: PART 1 — OSCILLATORY FLOW

Fulvio Stella
Dipartimento di Meccanica e Aeronautica, Universita di Roma "La Sapienza," Via Eudossiana 18, 00184 Rome, Italy

Edoardo Bucchignani
CIRA, Via Maiorise, 81043 Capua (CE), Italy

Transition from the steady state to an oscillatory regime in three-dimensional limited aspect ratio boxes, filled with an incompressible fluid and heated from below, has been examined by direct numerical simulation. Two different physical problems have been considered: the first is related to a domain 3.5× 1× 2.1 filled with water at 70°C (Prandtl number 2.5); the second considers a domain 2.4× 1× 1.2 filled with water at 33°C (Prandtl number 5). The Rayleigh number has been varied from 20,000 to 80,000. A new procedure based on a statistical approach for evaluation of the critical Rayleigh number for transition from steady state to oscillatory flow (Ra_{II}) has been introduced in order to reduce numerical errors and estimate the error bars. A systematic study for the determination of Ra_{II} has been conducted as a function of the geometries considered and the different flow structures observed.

INTRODUCTION

For the past century, Rayleigh-Bénard convection has been the subject of very intensive theoretical, experimental, and numerical studies. Analysis of the Rayleigh-Bénard problem is of practical importance for many engineering applications (e.g., thermal comfort, crystal growth, solar collectors). However, the main interest to researchers for this problem is theoretical, since Rayleigh-Bénard convection presents, during the evolution from the stationary state to the fully developed turbulent regime, such a rich scenario of different structures and sequences of bifurcations that it is widely considered a reference problem for the study of different transition mechanisms in fluid dynamics [1–3].

It is well-known that the main parameter that drives the physical phenomenon is the Rayleigh number (Ra). In fact, when Ra is lower than a first critical value Ra_I, the flow is stationary and heat transmission is only due to conduction. The value of Ra_I has been determined both analytically [4] and experimentally [5], being independent of the Prandtl number (Pr) and weakly dependent on the geometric aspect ratios of the domain: for a laterally unlimited

Received 27 July 1998; accepted 12 February 1999.

The authors would like to acknowledge Professor G. Guj to the University of Roma TRE for helpful suggestions provided in the development of this work. CIRA scpa (Capua) is also gratefully acknowledged for support during the development of the present work.

Address correspondence to Professor Fulvio Stella, Dipartimento di Meccanica e Aeronautica, Universita Degli Studi de Roma "La Sapienza," Via Eudossiana 18, 00184 Rome, Italy. E-mail: fulvio@stella.ing.uniroma1.it

NOMENCLATURE

b	right-hand side of linear systems	Δt	time step (nondimensional)
c	constant	ΔT	temperature jump
C	preconditioning matrix	Δx	spatial discretization step
f	oscillatory frequency (nondimensional)	Δy	spatial discretization step
g	gravitational acceleration	Δz	spatial discretization step
H	vertical size of the cavity	ε	generic parameter
L	horizontal size of the cavity	θ	temperature (nondimensional)
L	lower preconditioning matrix	κ	thermal diffusivity
n	normal to a surface	μ	condition number
n_i	number of grid points along x	ν	kinematic viscosity
n_j	number of grid points along y	σ	variance
n_k	number of grid points along z	Φ	phase of oscillation
Nu	Nusselt number	ω	vorticity component
Pr	Prandtl number ($= \nu/\kappa$)	$\boldsymbol{\omega}$	vorticity vector (nondimensional)
R	coefficient matrix		
Ra	Rayleigh number ($= g\beta\Delta TH^3/\kappa\nu$)		
S	generic surface	**Subscripts**	
t	time (nondimensional)		
T	period of oscillation	c	fixed value
u	component of velocity along x	i	counter
u	velocity vector (nondimensional)	max	maximum value
U	upper preconditioning matrix	min	minimum value
v	component of velocity along y	x	spatial coordinate
w	component of velocity along z	y	spatial coordinate
x	spatial coordinate	z	spatial coordinate
y	spatial coordinate	0	initial step
z	spatial coordinate	I	first critical number
β	coefficient of thermal expansion	II	second critical number

domain it is equal to 1708. As Ra becomes larger than $\mathrm{Ra_I}$, convective flows can be observed. The fluid motion is regular and organized as a set of horizontal parallel rolls (quasi-two-dimensional motion [4, 6]). An increase of Ra can cause the loss of stability of these configurations, which are replaced by fully three-dimensional configurations. As shown by many authors [7, 8], there are several instability mechanisms, such as *cross-roll*, bimodal convection, and *soft-roll*, dependent on Pr and on the wave number.

Moreover, a second transition, from steady to oscillatory flow, is observed when Ra is increased beyond the second critical Rayleigh number ($\mathrm{Ra_{II}}$). The flow is characterized by a sinusoidal wave traveling along the axes of the rolls, moving them alternately left and right.

Although oscillatory flow in the Rayleigh-Bénard problem has been observed by many authors, the determination of $\mathrm{Ra_{II}}$ has not yet been approached in a systematic way. In the present paper the authors intend to partially fill this gap, and the values of $\mathrm{Ra_{II}}$ found for the different geometries and flow structures under study are presented. In order to reduce procedural errors and obtain an a posteriori estimation of the numerical uncertainty, a statistical approach is applied in conjunction with the procedure introduced by LeQuere [9]. This approach has been preferred, in the present paper, to the one proposed by Griewank and

Reddien [10] because the latter is more complex from the computational point of view and is more sensitive to the initial approximations.

The physical system considered is a three-dimensional box, bounded by rigid and impermeable walls, filled with an incompressible Newtonian fluid, and heated from below. Vertical walls are adiabatic, while horizontal walls are isothermal and held at different temperatures. Two cases have been selected, which have already been the subject of experimental and numerical investigations. The first involves a domain $3.5 \times 1 \times 2.1$ (case A), filled with water at 70°C (Pr = 2.5). In order to compare and validate the numerical results, a configuration made up of two rolls orthogonal to the longest side wall of the box has been considered, similar to the experiments of Gollub and Benson [2] and the numerical simulations of Mukutmoni and Yang [11]. Further, an atypical configuration, made up of two rolls whose axes are not parallel (*soft-roll*), has been investigated.

The second case is a domain $2.4 \times 1 \times 1.2$ (case B), filled with water at 33°C (Pr = 5). For this problem, only the configuration with two rolls orthogonal to the longest horizontal side of the box has been considered.

The numerical code used in this work is based on the vorticity-velocity formulation of the Navier-Stokes equations [12] integrated in time by means of a fully implicit approach [13], with a preconditioned Bi-CGSTAB as linear system solver. The detection of types of instability and the study of their evolution in time are very sensitive to physical as well as numerical perturbations. For this reason a high accuracy has been achieved, and particular attention has been paid to reduce numerical noise and integration errors. The required accuracy has been obtained by using a large number of mesh points and a very small time step. Moreover, the numerical method adopted is critical in order to fully exploit, in terms of accuracy, the fine mesh and small time step used. All the numerical simulations have been conducted on the Convex Exemplar supercomputer with 16 processors.

MATHEMATICAL FORMULATION

Governing Equations

The governing equations for an incompressible Newtonian fluid with the Boussinesq approximation are formulated in terms of vorticity ω, velocity $\mathbf{u}$, and temperature θ:

$$\frac{1}{\mathrm{Pr}}\frac{\partial \omega}{\partial t} + \frac{1}{\mathrm{Pr}}\nabla \times (\omega \times \mathbf{u}) = \nabla^2 \omega - \mathrm{Ra}\nabla \times \left(\theta \frac{\mathbf{g}}{|g|}\right) \tag{1}$$

$$\nabla^2 \mathbf{u} = -\nabla \times \omega \tag{2}$$

$$\frac{\partial \theta}{\partial t} + (\mathbf{u} \cdot \nabla)\theta = \nabla^2 \theta \tag{3}$$

The nondimensional parameters Ra and Pr are defined as

$$\mathrm{Ra} = \frac{g\beta \Delta T H^3}{\kappa \nu} \qquad \mathrm{Pr} = \frac{\nu}{\kappa}$$

in which g is the gravitational acceleration, β is the coefficient of thermal expansion, ΔT is the temperature difference between hot and cold walls, H is the height of the box, κ is the thermal diffusivity, and ν is the kinematic viscosity. The nondimensional scheme is based on a reference velocity $\mathbf{u}^*$ defined as κ/H, a reference time t^* defined as H^2/κ, and in consequence, a reference frequency ($f^* = 1/t^*$) defined as κ/H^2. The vorticity ω is defined as usual:

$$\omega = \nabla \times \mathbf{u} \tag{4}$$

Boundary Conditions

The physical system considered is a three-dimensional box (L_x, 1, L_z) bounded by rigid, impermeable walls and heated from below. The vertical direction has been assumed to be coincident with the y axis. The horizontal walls are isothermal and held at different temperatures, while the vertical walls are adiabatic. The boundary conditions for the velocity are

$$u = v = w = 0$$

for all walls. The temperature boundary conditions are

$$\frac{\partial \theta}{\partial n} = 0 \qquad \begin{cases} x = 0 \\ x = L_x \\ z = 0 \\ z = L_z \end{cases}$$

$$\theta = 1 \qquad y = 0$$

$$\theta = 0 \qquad y = 1$$

The boundary condition associated with ω is the use of the vorticity definition on all the walls. So, for the vorticity components it must be

$$\omega_x = \frac{\partial w}{\partial u} - \frac{\partial v}{\partial z}$$

$$\omega_y = \frac{\partial u}{\partial z} - \frac{\partial w}{\partial x}$$

$$\omega_z = \frac{\partial v}{\partial x} - \frac{\partial u}{\partial y}$$

for all walls. This condition is essential for the conservation of the solenoidality of the vorticity field. As explained in the section below, Numerical Method, the governing equations, together with the boundary conditions, are solved coupled in a unique large linear system. So, for example, the boundary condition for ω_x is

solved in the following way:

$$\omega_x - \frac{\partial w}{\partial y} + \frac{\partial v}{\partial z} = 0$$

Heat Flux Evaluation

Heat flux, from the hot to the cold wall, has been evaluated using the proper definition of the mean Nusselt number on a horizontal section:

$$\mathrm{Nu} = \frac{1}{S}\int_S (\theta \mathbf{u} - \nabla\theta) \cdot \mathbf{n}\, dS$$

It is important to point out that if the flow is periodic, the reported quantities have been averaged over one period.

Initial Conditions

Two different geometries have been considered: the first (case A) is a domain with a $3.5 \times 1 \times 2.1$ geometry, filled with water at 70°C (Pr = 2.5); the second (case B) is a domain with a $2.4 \times 1 \times 1.2$ geometry, filled with water at 33°C (Pr = 5). In case A the first simulation has been executed at Ra = 20,000 starting from rest. Successively, Ra has been increased in steps of 1000, starting from the solution obtained at the previous value, up to Ra = 45,000. In case B the first simulation has been executed at Ra = 40,000 starting from rest. Successively, Ra has been increased in steps of 10,000, starting from the solution obtained at the previous value, up to Ra = 80,000. These values of step increase in Ra correspond to those chosen by Mukutmoni and Yang in analogous numerical simulations [14, 15].

A different approach has been adopted in the iterative procedure for the evaluation of $\mathrm{Ra}_{\mathrm{II}}$. Applying this procedure, all the solutions are oscillatory, with a nearly sinusoidal oscillation. Ra is decreased in small steps in order to approximate $\mathrm{Ra}_{\mathrm{II}}$. Other details are given in the section below, Evaluation of $\mathrm{Ra}_{\mathrm{II}}$.

NUMERICAL METHOD

The governing equations, Eqs. (1)–(3), together with the appropriate boundary conditions, have been discretized using a finite difference technique on a uniform Cartesian grid with $n_i \times n_j \times n_k$ points. Staggering of the variable locations has been chosen in order to obtain not only the maximum accuracy of the discretized terms, but also the discrete conservation of mass, vorticity, and thermal energy [12]. The location of the staggered variables is shown in Figure 1. Spatial derivatives have been discretized through second-order central differences, while time derivatives have been discretized through three-point second-order backward differences. Time integration has been executed by means of a fully implicit approach, in order to guarantee high stability to the method; such discretization

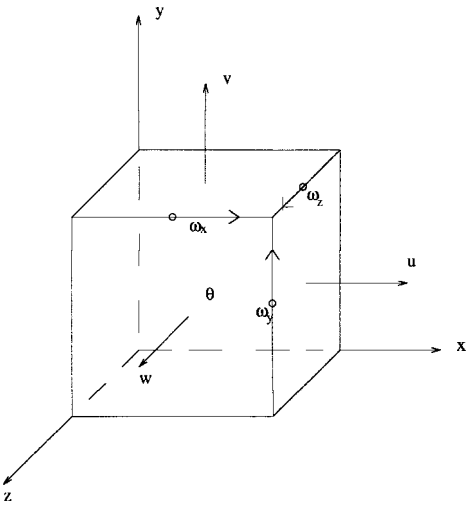

Figure 1. Computational molecule showing the 3-D staggered mesh.

gives rise to a system of nonlinear algebraic equations for each time step. It could be solved by decoupling the equations (as in the SIMPLEX algorithm [11]); however, we chose a procedure that ensures good coupling between the equations (frozen coefficients) in order to guarantee mass conservation and the definition of vorticity at each time step. High accuracy in the time integration is ensured [13]. The solenoidality of the vorticity field is identically satisfied in 2-D problems, while in 3-D it has to be enforced in some way. It has been demonstrated in Ref. [12] that the form of the advective term in Eq. (1) is essential for a straightforward satisfaction of this constraint.

In this way, a large, sparse linear system of equations $\mathbf{R}\,x = b$ has to be solved at each time step. The solution of these linear systems via a direct method is not recommended because of the size of the problem, so an iterative procedure has been preferred. A parallel implementation of the Bi-CGSTAB algorithm [16], associated with a block decomposition (BILU) of the matrix $\mathbf{R}$ as preconditioner [17], has been employed. This approach has the advantage of allowing great flexibility in writing the discretized form of the numerical model. The Bi-CGSTAB algorithm is an iterative method belonging to the class of Krylov subspace methods. It has been chosen for its good numerical stability and speed of convergence. The use of a preconditioning technique is, in all practical applications, essential to fulfill the stability and convergence requirements of the iterative procedure itself. The aim of the preconditioner is to convert the original linear system to an equivalent but better-conditioned system. This consists of finding a real matrix C such that $\mu(C^{-1}\mathbf{R}) < \mu(\mathbf{R})$ (μ is the condition number, i.e., the ratio between the maximum and the minimum eigenvalue). In this way, the new linear system

$$C^{-1}\mathbf{R}\,x = C^{-1}b$$

has (by design) better convergence and stability characteristics than the original system. One of the most widely used preconditioners is based on the Incomplete

Cholesky Factorization (ILU): the C matrix is defined as the product **LU** of a lower (**L**) and an upper (**U**) triangular matrix generated by means of a factorization of **R**. In order to perform parallel simulations, we adopted as preconditioner a modified version of ILU, called BILU, in which each processor performs a local ILU factorization only on the square block of its competence. Further details of the numerical method can be found in Refs. [12, 13]. All the numerical simulations have been conducted on the Convex Exemplar supercomputer. It consists of two hypernodes, each of which has 8 HP PA-RISC 7100 chips and up to 2 Gbytes of physical memory. The aggregate peak performance is about 3.2 GFlops.

Mesh Accuracy Evaluation

The code has been validated with the numerical results of Mukutmoni and Yang [11] for case A, assuming Ra = 20,000, with a configuration made up of two parallel rolls. Three grids have been used: $24 \times 14 \times 15$, $36 \times 21 \times 22$, and $54 \times 31 \times 32$. The maximum values of the three components of velocity and the Nusselt number in the vertical direction have been chosen for comparison. As proposed by de Vahl Davis [18], $\mathbf{u}_{max}$, $\mathbf{v}_{max}$, and $\mathbf{w}_{max}$ are computed by numerical differentiation through a fourth-order polynomial approximation, for better evaluation of the maximum values.

Results are reported in Table 1, showing good agreement with those of Mukutmoni and Yang [11]. The convergence analysis indicates that the method is nearly second-order accurate in space. In addition, the $36 \times 21 \times 22$ grid provides a solution that is accurate enough for the purposes of the paper, and therefore it has been used as a working grid for the other simulations related to this domain.

It is also important to provide a comparison of the numerical results with experimental data. For this reason, we performed a comparison of our results with those of Gollub and Benson [2] for case A at Ra = 30,000, assuming a configuration made up of two horizontal rolls (2T). Figure 2. shows the component of velocity along x as a function of x at $y = 0.875$ and $z = 1.65$ superimposed on the results of Gollub and Benson: good agreement is illustrated.

Table 1. Mesh sensitivity analysis: case A, configuration 2T, Ra = 20,000

	Grid size			
	$24 \times 14 \times 15$	$36 \times 21 \times 22$	$54 \times 31 \times 32$	Reference value
$\mathbf{u}_{max}$	42.954 (0.15%)	42.974 (0.10%)	42.975 (0.10%)	43.02
x, y, z	2.587, 0.228, 0.675	2.501, 0.215, 0.650	2.443, 0.204, 0.575	—
$\mathbf{v}_{max}$	54.420 (4.02%)	53.435 (2.25%)	52.945 (1.35%)	52.23
x, y, z	1.902, 0.538, 1.124	1.850, 0.466, 1.150	1.816, 0.472, 1.117	—
$\mathbf{w}_{max}$	8.421 (2.62%)	8.383 (2.18%)	8.364 (1.96%)	8.20
x, y, z	1.902, 0.884, 0.450	1.850, 0.842, 0.400	1.816, 0.820, 0.304	—
Nu	2.6926 (4.70%)	2.6222 (2.14%)	2.5916 (0.98%)	2.566

Reference values are those by Mukutmoni and Yang. Percentage differences are shown in parentheses.

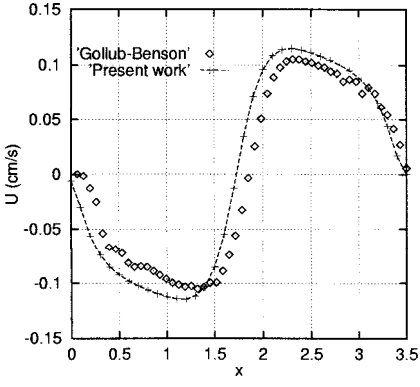

Figure 2. Case A, configuration 2T, Ra = 30,000. Component of velocity along x as a function of x at $y = 0.875$ and $z = 1.65$. Velocity is expressed in cm s^{-1}. Comparison with the results of Gollub and Benson [2] is shown.

The time step sensitivity analysis has been executed for case B assuming Ra = 80,000. As described in the section below, case B, at this value of Ra the flow is oscillatory periodic. The results are reported in Table 2. in terms of frequency and maximum and minimum values of u and v at point (0.7, 0.7, 0.7) for three different time steps. The analysis of results shows, surprisingly, an accuracy in time higher than second order.

Evaluation of Ra_{II}

Transition to unsteady convection is a key issue in the study of the Rayleigh-Bénard problem. For this reason, it is relevant to achieve a careful evaluation of Ra_{II} for each of the geometries and flow structures under study. Assuming that the onset of unsteady solutions is due to Hopf bifurcations, as is also suggested by experimental observation, different computational techniques may be adopted in order to determine Ra_{II}. A very accurate procedure has been defined by Griewank and Reddien [10], which has been successfully applied by Winters [19] to an analogous 2-D problem. However, this procedure is impractical if applied to 3-D problems. For this reason, in this work, another procedure, already used by LeQuere [9], has been considered and is here described.

Let ε be a parameter that drives the system (for example, the Rayleigh number). If for ε_c (a fixed value of ε) the kind of solution changes, ε_c is called a bifurcation point. In the specific case of the Navier-Stokes equations, Eqs. (1)–(3), a bifurcation point causing the transition from the steady state to an oscillatory

Table 2. Time step sensitivity analysis: case B, configuration 2T, Ra = 80,000

	$\Delta t = 10^{-4}$	$\Delta t = 5 \times 10^{-5}$	$\Delta t = 2.5 \times 10^{-5}$
f	34.180	34.158	34.158
u_{max}	−48.795	−48.588	−48.537
u_{min}	−54.061	−54.112	−54.116
v_{max}	14.609	15.027	15.031
v_{min}	−4.310	−4.518	−4.524

regime is when $Ra = Ra_{II}$. As we have assumed that this is a Hopf bifurcation, as a consequence (as shown in Ref. [20]), for Ra slightly greater than Ra_{II}, the amplitude of oscillation in time of the velocity, vorticity, and temperature grows as $(Ra - Ra_{II})^{1/2}$:

$$X(t) = X_c + k(Ra - Ra_{II})^{1/2} \sin(2\pi ft + \phi) \qquad X = \{u_i, \omega_i, \theta\} \tag{5}$$

where X_c is the solution at the bifurcation point. The square root assumption for amplitude oscillation has been numerically verified a posteriori in order to guarantee the correctness of the hypothesis. In this view the solution at Ra_{II} can be defined as an oscillatory solution with zero amplitude of oscillation. The critical solution and the corresponding Ra_{II} can be determined by using the amplitude of oscillation of the solutions found in correspondence of two overestimations (Ra_a and Ra_b in Table 3) of the critical Ra and extrapolating the new critical value. The procedure has to be repeated iteratively, solving at each iteration one oscillatory flow field at a Rayleigh number intermediate between the critical Ra at the previous iteration and the minimum of Ra_a and Ra_b. It is important to observe that in this way the critical value Ra_{II} related to the base solution X_c of Eq. (5) is found. Since different base solutions X_c lead to different values of Ra_{II}, it is crucial for the correct application of the procedure that at the different steps of the method the base solution X_c is maintained the same for the various oscillatory solutions evaluated. (As different base solutions, they have to be considered not only solutions with different flow patterns, e.g., 2T, SR, but also solutions having the same flow pattern with minor differences, such as rolls, deformations, bubbles.) Since the step in Ra adopted for approximating Ra_{II} is usually small (see Table 3), in the present paper this result has been obtained adopting as an initial guess the solution at Ra_b found at the previous approximation step.

Moreover, it is worth noting that, because of the nonlinearity of the problem, the finite amplitude oscillations considered in Eq. (5) for each single variable lead to slightly different values of the extrapolated Ra_{II}. For this reason, a statistical procedure has been adopted, obtaining also an evaluation of the numerical error. Several points in the grid have been randomly chosen, and the values of 100 variables have been tracked during one complete period, determining the amplitude of oscillation. Ra_{II} has been evaluated for each of these variables. As an

Table 3. Sequence of approximations obtained for the evaluation of Ra_{II}: case B, configuration 2T

Ra_a	Ra_b	Ra_{II}	σ
58,000	55,000	46,623	1856
55,000	51,000	45,533	1603
51,000	49,000	45,158	939
49,000	47,000	44,548	484
47,000	45,500	44,202	203
45,500	44,800	44,150	80

Table 4. Values of Ra_{II} for the selected cases

Domain	Pr	Configuration	Ra_{II}	σ
$3.5 \times 1 \times 2.1$	2.5	2T	34,120	305
$3.5 \times 1 \times 2.1$	2.5	SR	37,960	5
$2.4 \times 1 \times 1.2$	5.	2T	44,150	80

example of the effectiveness of the method, in Table 3 the results in terms of averaged value and variance σ,

$$\sigma = \left(\frac{\Sigma_i (x_i - \bar{x})^2}{n^2} \right)^{1/2}$$

are reported for different pairs of Ra_a and Ra_b. The test case considered is the one described in the section below, Case B. It is evident that the error can be reduced as required by the problem under study, by reducing iteratively the distance of Ra_a and Ra_b from the estimated Ra_{II}. In the following, the estimated errors have been assumed to be equal to σ. It is worth observing that in the first row of Table 3 the value obtained for Ra_{II} appears very inaccurate when compared with the final value found for Ra_{II} (44,150). For this case, even considering the uncertainty assumed for the method equal to σ (1856), the final result is not included in the error bar. This anomaly is due to the nonlinearity of the Navier-Stokes equations and to the large distance, in terms of Ra, of the initial guess for Ra_a and Ra_b.

A summary of all the values of Ra_{II} for the cases presented in the next section is reported in Table 4.

RESULTS

Case A: $3.5 \times 1 \times 2.1$, Pr = 2.5

As discussed in above, a grid with $36 \times 21 \times 22$ points has been used for the spatial discretization ($\Delta x = \Delta z = 0.1$, $\Delta y = 0.05$). The time step has been set equal to 10^{-3}, as a good compromise between time-accuracy and computational resources. As shown by many authors [6–8], for Ra greater than the first critical value Ra_I, under the same conditions, the Navier-Stokes equations may have more than one solution. The several solutions can be classified following the nomenclature adopted in Ref. [7]:

1. Quasi two-dimensional pattern in the form of rectilinear rolls consisting of

   - n transverse rolls (nT), n being an integer, which are orthogonal to the longest side wall of the box
   - n longitudinal rolls (nL), which are parallel to the longest side wall of the box

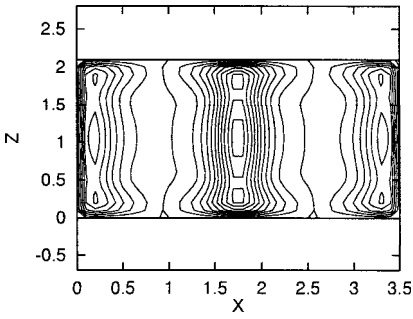

Figure 3. Case A, Ra = 20,000. Isolines of the vertical component of velocity in the horizontal middle plane. A configuration made up of two horizontal parallel rolls (2T) is observed.

2. Fully three-dimensional flow caused by

   - bimodal convection, consisting of a base flow superimposed with cross-rolls of approximately the same strength as the base flow
   - distortion of the original rolls into an L shape. This configuration, called soft-roll, allows a continuous transition between different wave number flow patterns

In fact, for Ra = 20,000 we found two different steady and stable configurations. The first is made up of two rolls with axes orthogonal to the longest side wall of the box (2T). The initial 2T flow structure has been obtained by imposing a cold ($\theta = 0$) rectangular narrow region in the middle of the hot wall for a short time interval at the beginning of the numerical simulation. Isocurves of the vertical velocity component in the horizontal middle plane are shown in Figure 3. The second flow configuration is made up of two rolls whose axes are not parallel (*soft-roll* configuration; see Figure 5), which has been obtained starting from rest, without imposing any disturbance (e.g., the cold region).

Configuration 2T. Starting from configuration 2T obtained at Ra = 20,000, Ra has been increased in steps of 1000. Table 5 reports the main frequency and the average Nusselt number in the vertical direction as a function of Ra. Up to 34,000, the flow is steady, and the configuration does not change. Instead, at Ra = 35,000 an unsteady periodic flow with a fundamental frequency was found. Following the procedure described in the previous section, Ra_{II} has been determined: in this case it is equal to 34,120 ± 305. This result is an overestimation of about 15% with respect to the results of Gollub and Benson [2] and Mukutmoni and Yang [11]. It is

Table 5. Case A, configuration 2T: Main frequency, average Nusselt number in vertical direction as a function of Ra

Ra	f	$\overline{Nu}$
20,000	steady	2.622
30,000	steady	2.905
35,000	15.136	3.020
40,000	16.601	3.236
45,000	17.578	3.340

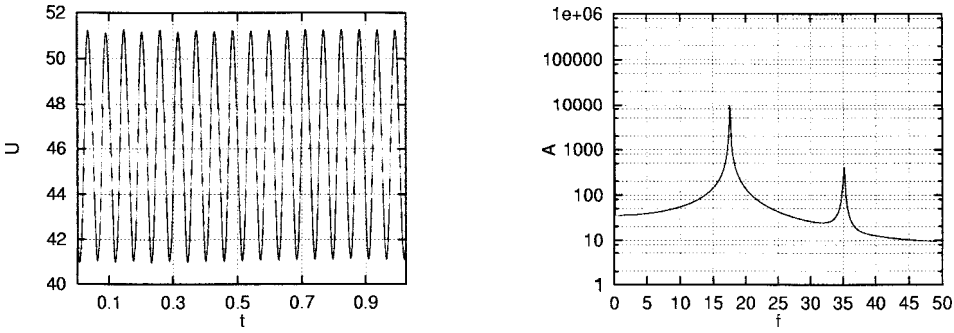

Figure 4. Case A, configuration 2T, Ra = 45,000. Time history of the component of velocity along x at point (0.7, 0.7, 0.7) (*left*) and FFT of this signal (*right*). A periodic flow regime with a fundamental frequency $f = 17.578$ and its harmonics is illustrated.

worth observing that the results presented here were obtained by means of a very accurate time integration method (see section above, Numerical Method) and an ad hoc procedure for approaching $\mathrm{Ra}_{\mathrm{II}}$. Since the main goal of the above studies was not a very accurate determination of $\mathrm{Ra}_{\mathrm{II}}$, these differences may be explained as a consequence of the more coarse procedure adopted there and the result of the difficulties in determining very small amplitude oscillations.

Up to Ra = 45,000 there is no qualitative change in the flow. The time history of the component of velocity along x at point (0.7, 0.7, 0.7) looks sinusoidal. A frequency analysis, obtained by fast Fourier transform (FFT), executed on 8192 points (frequency resolution $\Delta f = 1/T_0 = 0.122$, 1000 samples for each unit of nondimensional time), shows that the main frequency f is equal to 17.578. (All the FFT presented in this paper have been executed on 8192 points.) It is accompanied by a harmonic frequency, equal to $2f$. Figure 4 shows the time history of the component of velocity along x at point (0.7, 0.7, 0.7) and the FFT of this signal. The further evolution of the system at higher Ra is discussed in the companion paper (Bucchignani and Stella, this issue).

Soft-roll configuration. The second steady solution we found in Ra = 20,000 is a *soft-roll* configuration. It is nonsymmetric, as the axes of the two rolls are not parallel. Figure 5 shows the isocurves of the vertical velocity component in

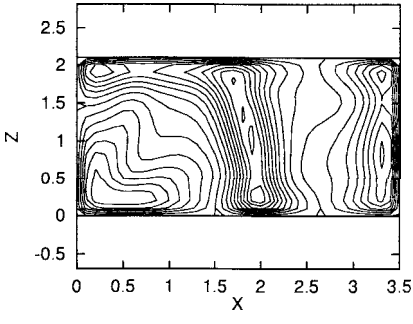

Figure 5. Case A, Ra = 20,000. Isolines of the vertical component of velocity in the horizontal middle plane. A fully three-dimensional configuration (*soft-roll*) made up of two horizontal rolls whose axes are not parallel is observed.

Table 6. Case A, *soft-roll* configuration: Main frequency, average Nusselt number in vertical direction as a function of Ra

Ra	f	$\overline{\mathrm{Nu}}$
20,000	steady	2.632
30,000	steady	2.942
36,000	steady	3.099
38,000	4.975	3.144
45,000	5.615	3.351

the horizontal middle plane. Such a configuration has already been observed experimentally by Kolodner et al. [8] and numerically by Stella et al. [7] in larger domains. On the other hand, it was not observed by Mukutmoni and Yang [11, 14] or by Gollub and Benson [2], so we have no results for comparison. The stability of this solution has been verified by applying a small random perturbation to the vorticity field. After a short time, the solution goes back to the original *soft-roll* configuration, with the same numerical values. Starting from the solution obtained at Ra = 20,000, we increased Ra in steps of 1000. Table 6 reports the main frequency and the average Nusselt number in the vertical direction as a function of Ra. An unsteady periodic flow with a fundamental frequency ($f = 4.975$) was found for Ra = 38,000. In this case, $\mathrm{Ra}_{\mathrm{II}} = 37{,}960 \pm 5$, which is a bit larger than the previous case, emphasizing that it depends on the type of configuration. Up to Ra = 45,000, the flow remains periodic. Figure 6 shows the time history of the component of velocity along x at point (0.7, 0.7, 0.7) and the FFT of this signal. Further increases in Ra cause substantial changes in the temporal regime, which is discussed in the companion paper (Bucchignani & Stella, this issue).

Case B: $2.4 \times 1 \times 1.2$, Pr = 5

Case B has also been investigated by Mukutmoni and Yang [15], who considered a fluid dynamical configuration made up of two parallel rolls. Following

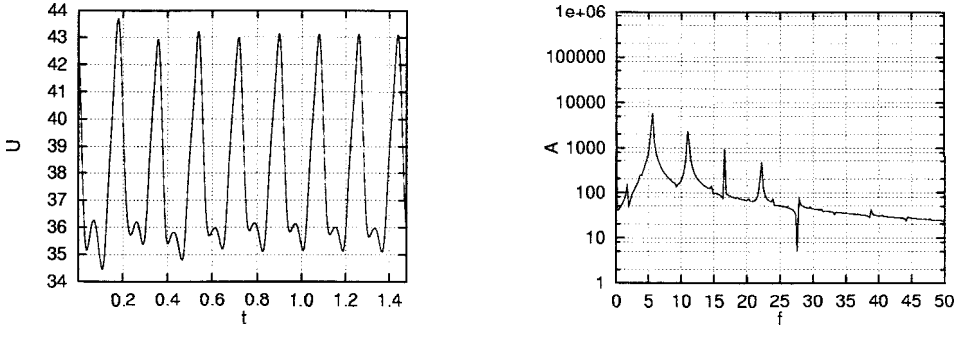

Figure 6. Case A, *soft-roll*, Ra = 45,000. Time history of the component of velocity along x at point (0.7, 0.7, 0.7) (*left*) and FFT of this signal (*right*). Periodic flow regime with a fundamental frequency $f = 5.615$ and its harmonics is illustrated.

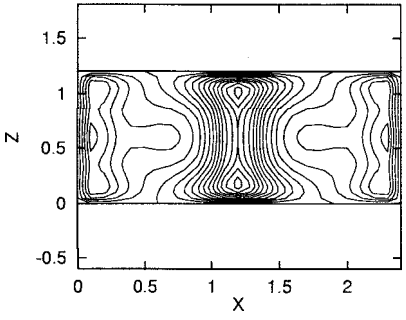

Figure 7. Case B, Ra = 40,000. Isolines of the vertical component of velocity in the horizontal middle plane. A configuration made up of two horizontal parallel rolls (2T) is observed.

their indications, a grid with $25 \times 21 \times 25$ points ($\Delta x = 0.1$, $\Delta y = \Delta z = 0.05$) has been used, while Δt has been set equal to 10^{-4}. The first simulation was executed at Ra = 40,000, which gave rise to a steady and stable flow made up of two parallel rolls (2T) (Figure 7), in good qualitative agreement with that found by Mukutmoni and Yang [15]. From this solution, Ra has been increased in steps of 10,000. Table 7 reports the main frequency and the average Nu in the vertical direction as a function of Ra. At Ra = 50,000 the flow is oscillatory with a fundamental frequency $f = 26.855$. In this case, $\mathrm{Ra}_{\mathrm{II}} = 44{,}150 \pm 80$, showing an underestimation of about 12% with respect to the numerical finding of Mukutmoni and Yang [15]. The flow remains periodic up to Ra = 80,000. Figure 8 shows the time history of the component of velocity along x at point (0.7, 0.7, 0.7) and the frequency analysis obtained by FFT of this signal (frequency resolution $\Delta f = 1/T_0 = 1.22$, 10,000 samples for each unit of nondimensional time). The further evolution of the system is discussed in the companion paper (Bucchignani & Stella, this issue).

CONCLUSIONS

A numerical study of transition from steady to unsteady flow in Rayleigh-Bénard convection in limited domains has been performed by means of a parallel, fully implicit method. The main goal of the paper is to apply a new statistical approach for the determination of $\mathrm{Ra}_{\mathrm{II}}$. The procedure adopted allows not only the determination of the critical value of Ra but also an evaluation of its uncertainty. It has been shown that the uncertainty can be reduced as required in the specific problem under investigation by applying the proposed procedure iteratively. The method has been applied to a number of different cases, showing a

Table 7. Case B, configuration 2T: Main frequency, average Nusselt number in vertical direction as a function of Ra

Ra	f	$\overline{\mathrm{Nu}}$
40,000	steady	3.240
50,000	26.855	3.468
60,000	29.290	3.793
80,000	34.180	4.080

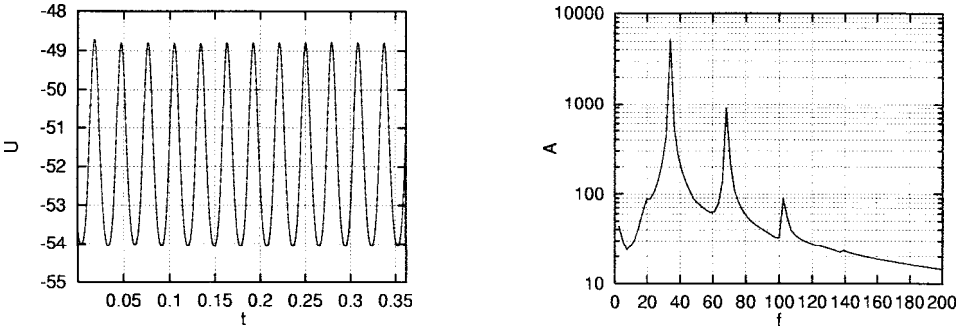

Figure 8. Case B, configuration 2T, Ra = 80,000. Time history of the component of velocity along x at point (0.7, 0.7, 0.7) (*left*) and FFT of this signal (*right*). Periodic flow regime with a fundamental frequency $f = 34.180$ and its harmonics is illustrated.

strong dependence of Ra_{II} on the problem parameters (Pr, aspect ratio) and on the fluid flow configurations. When possible, the obtained values of Ra_{II} have been compared with those available in the literature, showing non-negligible differences of about 12%–15%. Because of the difficulties related to this type of investigation, using both numerical and experimental approaches, not many results are available in the literature for a comparison. So, although the method used in the present paper seems very robust, it is not possible to determine the reasons for these differences more clearly.

Other results in terms of oscillation frequencies and Nu near the critical point have also been presented. Further interesting evolutions of the system as Ra is increased are presented in the companion paper (Bucchignani & Stella, this issue).

REFERENCES

1. R. M. Clever, and F. H. Busse, Transition to Time-Dependent Convection, *J. Fluid Mech.*, vol. 65, pp. 625–645, 1974.
2. J. P. Gollub and S. V. Benson, Many Routes to Turbulent Convection, *J. Fluid Mech.*, vol. 100, pp. 449–470, 1980.
3. J. H. Curry, J. R. Herring, J. Loncaric, and S. A. Orzag, Order and Disorder in Two- and Three-Dimensional Bénard Convection, *J. Fluid Mech.*, vol. 147, pp. 1–38, 1984.
4. S. Davis, Convection in a Box: Linear Theory, *J. Fluid Mech.*, vol. 30, no. 3, pp. 465–478, 1967.
5. K. Stork and U. Muller, Convection in a Box: Experiments, *J. Fluid Mech.*, vol. 54, no. 4, pp. 599–611, 1972.
6. F. H. Busse, Non-Stationary Finite Amplitude Convection, *J. Fluid Mech.*, vol. 28, pp. 223–239, 1967.
7. F. Stella, G. Guj, and E. Leonardi, The Rayleigh Benard Problem in Intermediate Bounded Domain, *J. Fluid Mech.*, vol. 254, pp. 375–400, 1993.
8. P. Kolodner, R. Walden, A. Passner, and C. Surko, Rayleigh-Benard Convection in an Intermediate Aspect Ratio Rectangular Container, *J. Fluid Mech.*, vol. 163, pp. 195–226, 1986.

9. P. LeQuere, Contribution to the GAMM-Workshop with a Chebyshev Collocation Scheme on a Staggered Grid, *Notes Numer. Fluid Mech.*, vol. 27, pp. 227–236, 1990.
10. A. Griewank and G. Reddien, The Calculation of Hopf Points by a Direct Method, *IMA J. Numer. Anal.*, vol. 3, pp. 295–303, 1983.
11. D. Mukutmoni and K. T. Yang, Raleigh-Bénard Convection in a Small Aspect Ratio Enclosure: Part I—Bifurcation to Oscillatory Convection, *J. Heat Transfer*, vol. 115, pp. 360–366, 1993.
12. G. Guj and F. Stella, A Vorticity-Velocity Method for the Numerical Solution of 3D Incompressible Flows, *J. Comput. Phys.*, vol. 106, pp. 286–298, 1993.
13. F. Stella and E. Bucchignani, True Transient Vorticity-Velocity Method Using Preconditioned Bi-CGSTAB, *Numer. Heat Transfer Part B*, vol. 30, pp. 315–339, 1996.
14. D. Mukutmoni and K. T. Yang, Rayleigh Bénard Convection in a Small Aspect Ratio Enclosure: Part II—Bifurcation to Chaos, *J. Heat Transfer*, vol. 115, pp. 367–376, 1993.
15. D. Mukutmoni and K. T. Yang, Thermal Convection in Small Enclosures: An Atypical Bifurcation Sequence, *Int. J. Heat Mass Transfer*, vol. 38, no. 1, pp. 113–126, 1995.
16. H. van der Vorst, Bi-CGSTAB: A Fast and Smoothly Converging Variant of Bi-CG for the Solution of Nonsymmetric Linear Systems, *SIAM J Sci. Stat. Comput.*, vol. 13, no. 2, pp. 631–644, 1992.
17. F. Stella, M. Marrone, and E. Bucchignani, A Parallel Preconditioned CG Type Method for Incompressible Navier-Stokes Equations, in A. Ecer et al. (eds.), *Parallel Computational Fluid Dynamics: New Trends and Advances*, pp. 325–332, Elsevier, Amsterdam, 1993.
18. G. de Vahl Davis, Natural Convection of Air in a Square Cavity: A Bench Mark Numerical Solution, *Int. J. Numer. Methods Fluids*, vol. 3, pp. 249–264, 1983.
19. K. Winters, Oscillatory Convection in Liquid Metals in a Horizontal Temperature Gradient, *Int. J. Methods Eng.*, vol. 25, pp. 401–414, 1988.
20. D. D. Joseph, *Stability of Fluid Motion*, vol. 1, Springer-Verlag, New York, 1976.